Received: 25 May 2020 | Revised: 29 July 2020

DOI: 10.1111/mmi.14585

RESEARCH ARTICLE

WILEY

The phytopathogen *Xanthomonas campestris* utilizes the divergently transcribed *pobA/pobR* locus for 4-hydroxybenzoic acid recognition and degradation to promote virulence

Bo Chen[1] | **Rui-Fang Li**[2] | **Lian Zhou**[3] | **Jia-Hui Qiu**[1] | **Kai Song**[1] | **Ji-Liang Tang**[4] | **Ya-Wen He**[1]

[1]State Key Laboratory of Microbial Metabolism, Joint International Research Laboratory of Metabolic and Developmental Sciences, School of Life Sciences and Biotechnology, Shanghai Jiao Tong University, Shanghai, China

[2]Guangxi Key Laboratory of Biology for Crop Diseases and Insect Pests, Plant Protection Research Institute, Guangxi Academy of Agricultural Sciences, Nanning, China

[3]Zhiyuan Innovation Research Centre, Student Innovation Institute, Zhiyuan College, Shanghai Jiao Tong University, Shanghai, China

[4]State Key Laboratory for Conservation and Utilization of Subtropical Agro-Bioresources, College of Life Science and Technology, Guangxi University, Nanning, China

Correspondence
Ya-Wen He, State Key Laboratory of Microbial Metabolism, Joint International Research Laboratory of Metabolic and Developmental Sciences, School of Life Sciences and Biotechnology, Shanghai Jiao Tong University, Shanghai 200240, China.
Email: yawenhe@sjtu.edu.cn

Funding information
National Key R&D Program of China, Grant/Award Number: 2017YFD0200900; National Natural Science Foundation of China, Grant/Award Number: 31972231 and 31772121

Abstract

Xanthomonas campestris pv. *campestris* (*Xcc*) is the causal agent of black rot in crucifers. Our previous findings revealed that *Xcc* can degrade 4-hydroxybenzoic acid (4-HBA) via the β-ketoadipate pathway. This present study expands on this knowledge in several ways. First, we show that infective *Xcc* cells induce in situ biosynthesis of 4-HBA in host plants, and *Xcc* can efficiently degrade 4-HBA via the *pobA/pobR* locus, which encodes a 4-hydroxybenzoate hydroxylase and an AraC-family transcription factor respectively. Next, the transcription of *pobA* is specifically induced by 4-HBA and is positively regulated by PobR, which is constitutively expressed in *Xcc*. 4-HBA directly binds to PobR dimers, resulting in activation of *pobA* expression. Point mutation and subsequent isothermal titration calorimetry and size exclusion chromatography analysis identified nine key conserved residues required for 4-HBA binding and/or dimerization of PobR. Furthermore, overlapping promoters harboring fully overlapping −35 elements were identified between the divergently transcribed *pobA* and *pobR*. The 4-HBA/PobR dimer complex specifically binds to a 25-bp site, which encompasses the −35 elements shared by the overlapping promoters. Finally, GUS histochemical staining and subsequent quantitative assay showed that both *pobA* and *pobR* genes are transcribed during *Xcc* infection of Chinese radish, and the strain Δ*pobR* exhibited compromised virulence in Chinese radish. These findings suggest that the ability of *Xcc* to survive the 4-HBA stress might be important for its successful colonization of host plants.

KEYWORDS
4-hydroxybenzoic acid, pathogenicity, *pobA*, *pobR*, *Xanthomonas campestris*

1 | INTRODUCTION

Xanthomonas campestris pv. *campestris* (Pammel) Dowson (*Xcc*) is the causal agent of black rot in crucifers. Black rot is a destructive disease associated with the cabbage family and has been reported in over 90 countries across the five continents (Vicente and Holub, 2013). Due to its importance in agriculture and deep understanding of virulence and plant-pathogen interactions (Büttner and Bonas, 2010; Zhou *et al*., 2017; Timilsina *et al*., 2020), *Xcc* is one of the top 10 plant pathogenic bacteria in molecular plant pathology (Mansfield *et al*., 2012) and is also a powerful model for research toward solutions in disease control (Timilsina *et al*., 2020).

Xcc has at least two distinctly unique in vivo life cycle stages: an epiphytic stage that occurs on plant surfaces and a pathogenic stage that occurs within the plant (Hugouvieux *et al*., 1998). During infection inside the host plant, 4-hydroxybenzoic acid (4-HBA)

represents one of the key stresses that the pathogen encounters. The multiple degradative enzymes produced by *Xcc* not only cleave the cell wall to generate simple sugars, but also release lignin, which, when hydrolyzed, forms various types of aromatics such as 4-HBA, ferulic acid, vanillic acid and *p*-coumaric acid (Bertani *et al*., 2001). *p*-coumaric acid can be further degraded into 4-HBA by microorganisms via at least three pathways (Venturi *et al*., 1998; Jung *et al*., 2016). Moreover, 4-HBA is reported to be one of the most important phenolics in plant defense responses against pathogen attack. Biosynthesis of 4-HBA in cell cultures of carrot and potato can be promoted following treatment with pathogenic fungal elicitors (Sircar and Mitra, 2008). In response to pathogenic attack, a range of broad-spectrum antimicrobial phenolics, including salicylic acid (2-HBA) and 4-HBA, are synthesized de novo and accumulated rapidly at areas of pathogen infection in *Brassica* plants. Following accumulation, the antimicrobial phenolics act to puncture the cell wall, delay maturation, disrupt metabolism or prevent reproduction of the pathogen (Glazebrook and Ausubel, 1994; Tan *et al*., 2004). It remains unclear how *Xcc* overcomes these phenolic stresses during infection.

4-HBA can be synthesized via different chorismatases from the end-product of the shikimate pathway. It serves as an important endogenous aromatic ring precursor for a wide range of primary and secondary metabolites in higher organisms (Grüninger *et al*., 2019). In nature, 4-HBA can be produced from fossil-fuel consumption. Bacteria and fungi represent the most important recyclers of aromatic compounds of both natural and human origins (Fuchs *et al*., 2011). In bacteria, catabolism of 4-HBA by dioxygenases is mediated by either the *ortho* cleavage (β-ketoadipate pathway) or *meta* cleavage pathways (Harwood and Parales, 1996; Romero-Silva *et al*., 2013). In the β-ketoadipate pathway, 4-HBA is hydroxylated by 4-HBA 3-hydroxylase (PobA) to yield protocatechuate (PCA), which is positively regulated by PobR in several environmental or rhizosphere bacterial species such as *Azotobacter chroococcum*, *Pseudomonas* sp., *Rhizobium leguminosarum*, *Acinetobacter calcoaceticus* and *Cupriavidus necator* (Dimarco and Ornston, 1994; Quinn *et al*., 2001; Donoso *et al*., 2011). However, the detailed molecular mechanisms underlying the induction of *pobA* expression by 4-HBA have yet to be identified.

Our previous findings revealed that the phytopathogen *Xcc* can convert 4-HBA and protocatechuate (PCA) into succinyl-CoA and acetyl-CoA via the β-ketoadipate pathway (Wang *et al*., 2015). Deletion of the gene encoding the key component of the β-ketoadipate pathway resulted in significantly reduced virulence in Chinese radish (He *et al*., 2006). These findings suggest that successful *Xcc* infection may be partially dependent on the catabolism of plant-derived aromatic compounds.

This current study initially analyzed the endogenous 4-HBA levels in *Xcc*-infected and uninfected cabbage and Chinese radish. The roles of the *pobR*/*pobA* locus in 4-HBA catabolism and the inductive expression patterns of both genes by 4-HBA were subsequently investigated. Genetic, biochemical and biophysical approaches were used to investigate the molecular mechanisms underlying PobR binding to 4-HBA and PobR dimerization; the composition of the

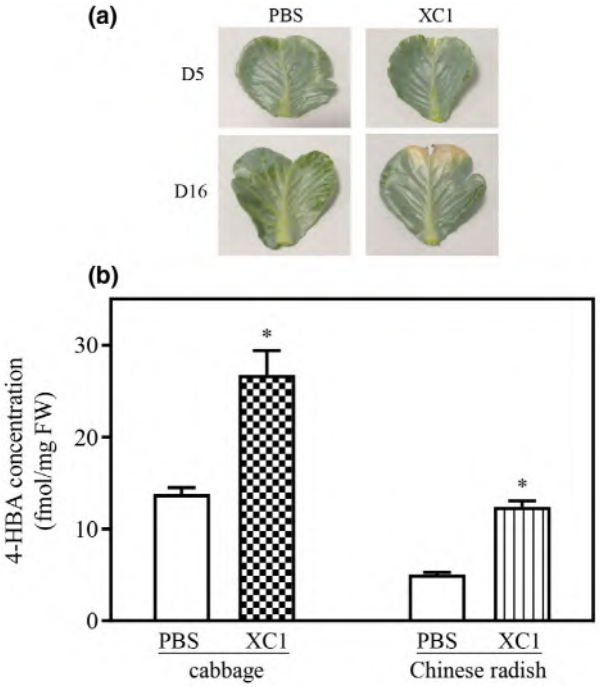

FIGURE 1 *Xcc* infection of host plants resulted in increased 4-HBA production. (a) Infected cabbage leaves at 5- and 16-days post inoculation. (b) Quantitative analysis of endogenous 4-HBA levels in the infected leaves of cabbage and Chinese radish at 5-days post inoculation by ultra-high performance liquid chromatography coupled with triple quadrupole tandem mass spectrometry. Fifteen leaves were inoculated with each tested strain or 1 × PBS buffer. Shown are the averages for three technical repeats with standard deviation. Statistically significant differences are indicated by one asterisk ($p \leq .05$) [Colour figure can be viewed at wileyonlinelibrary.com]

PobR binding sites in the overlapping promoters were also investigated. Finally, the expression of both *pobA* and *pobR* was investigated during *Xcc* infection inside Chinese radish. The findings suggest that 4-HBA utilization ability contributes to *Xcc* virulence in host plants.

2 | RESULTS

2.1 | Xcc infection promotes 4-HBA biosynthesis in cabbage and Chinese radish

In this study, 2-month mature leaves of cabbage and Chinese radish were infected by *Xcc* strain XC1 using the scissor clipping inoculation method. The negative control leaves were both wounded and inoculated with 1 × PBS buffer in the same manner as the XC1-treated plants. Clear infection lesions could be observed at 5-days post inoculation of XC1, and a total of 200 mg of 2.5 cm × 2.5 cm leaf squares were collected for 2-HBA, 3-HBA and 4-HBA extraction and quantitative analysis (Figures 1 and S1). As expected, the levels of 2-HBA in XC1-infected cabbage and Chinese radish leaves were much higher than those in control leaves (Figure S2a). XC1 infection also induces

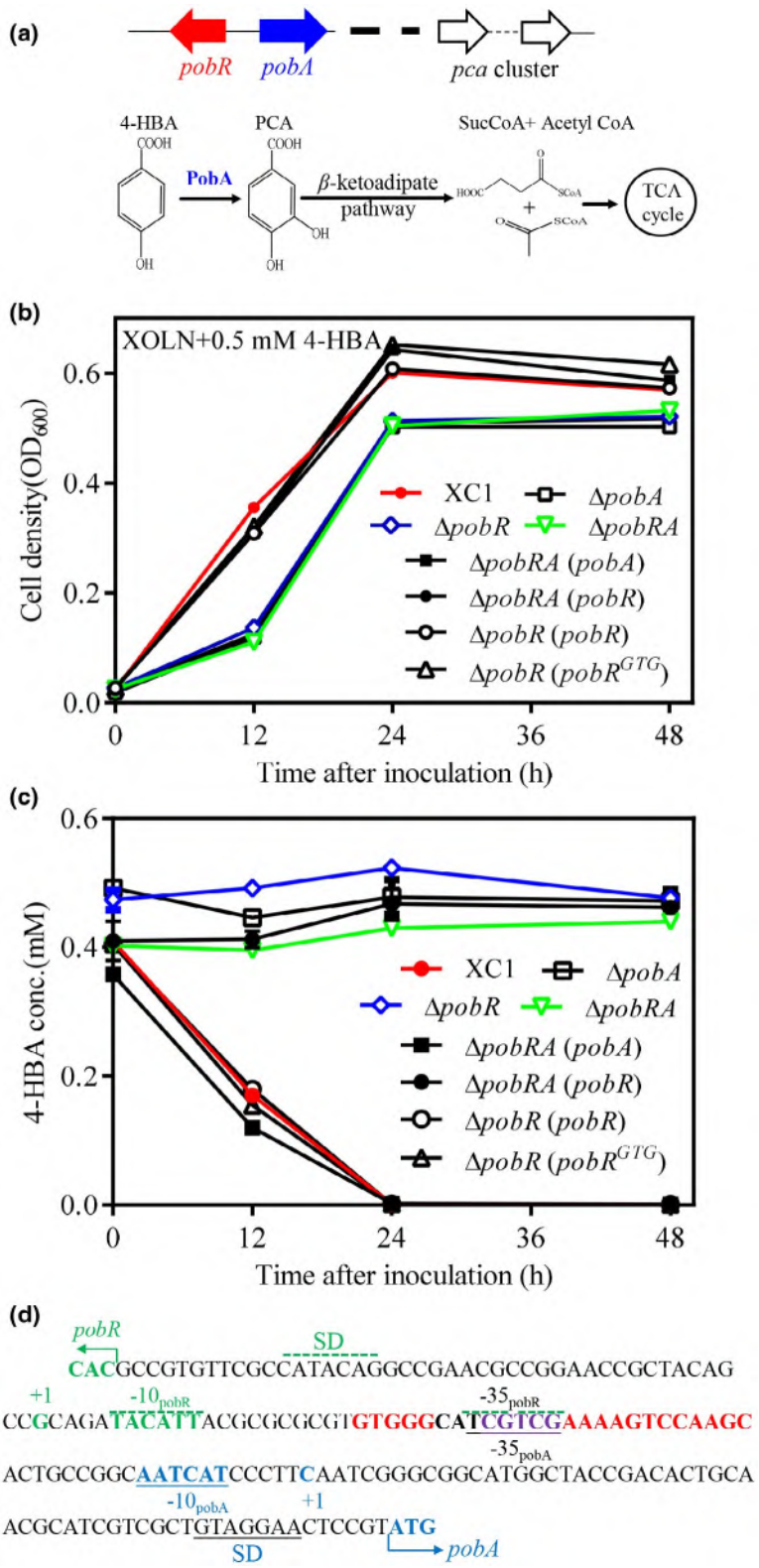

FIGURE 2 The *pobR/pobA* locus is required for 4-HBA catabolism in cell culture. (a) Genomic location of *pobR/pobA* locus and the general pathway for 4-HBA degradation in *Xcc*. PCA: protocatechuate. (b) Growth time course of XC1 and XC1-derived mutants in XOLN medium supplemented with 0.5 mM 4-HBA. (c) Time course of 4-HBA levels of XC1 and XC1-derived mutants in XOLN cultures. Shown are the averages for three technical repeats with standard deviation. (d) The overlapping promoters between the divergently transcribed *pobA* and *pobR* [Colour figure can be viewed at wileyonlinelibrary.com]

the production of higher levels of 4-HBA inside the infected leaves of both cabbage and Chinese radish. For example, 26.7 fmol mg^{-1} fresh weight (FW) 4-HBA was observed in the XC1-infected cabbage leaves, which is ca. 2.0-fold greater than the 13.7 fmol mg^{-1} FW observed for the control leaves (Figure 1). For 4-HBA, 12.3 fmol mg^{-1} FW was observed for the XC1-infected Chinese radish leaves, which is ca. 2.5-fold greater than the 5.0 fmol mg^{-1} FW observed for the control leave tissues (Figure 1). In contrast, XC1 infection did not have a significant effect on 3-HBA biosynthesis in the infected leaves of cabbage and Chinese radish (Figure S2b).

2.2 | The pobA/pobR locus is essential for 4-HBA degradation in XC1

When grown in XOLN medium supplemented with 0.5 mM 4-HBA, XC1 efficiently degraded 4-HBA (Figure 2c). A divergently transcribed *pobA-pobR* locus was identified seven genes upstream of the *pca* cluster (Figure 2a). *pobA* encodes a putative 4-hydroxybenzoate hydroxylase while *pobR* encodes for an AraC-family transcriptional regulator. To examine the possible involvement of *pobA-pobR* locus in 4-HBA degradation, a series of mutant strains were generated in XC1. When grown in basal XOLN medium supplemented with 0.5 mM 4-HBA, the mutant strains Δ*pobA* and Δ*pobR*, and *pobA* and *pobR* double deletion strain Δ*pobRA* displayed slower growth than the strain XC1 at 12 h post inoculation (hpi) (Figure 2b). Overexpression of *pobA* in strain Δ*pobRA* restored the growth defect. In contrast, overexpression of *pobR* in strain Δ*pobRA* had little effect on compromised bacterial growth (Figure 2b). 4-HBA levels declined over time and 4-HBA was not detectable in XC1 cultures after 24 hpi (Figure 2c). In contrast, 4-HBA levels remained constant in the cultures of the strains Δ*pobA*, Δ*pobR* and Δ*pobRA* during growth (Figure 2c). These results suggest that both *pobA* and *pobR* are essential for 4-HBA degradation. Overexpression of *pobA* in the double deletion mutant Δ*pobRA* restored 4-HBA degradation activity; however, overexpression of *pobR* had little effect on 4-HBA degradation (Figure 2c), suggesting that the 4-HBA hydroxylase PobA acts downstream of PobR during its involvement in 4-HBA degradation.

2.3 | Defining the overlapping promoters of pobA and pobR

The genomic information associated with the sequenced *Xcc* strains ATCC33913, 8,004 and B100 suggest that the intergenic region of *pobA* and *pobR* contains two divergent promoters, P_{pobA} and P_{pobR}(Figure 2d). It remains unclear how the two promoters are precisely organized. To this end, 5′-RACE was employed to identify the 5′-end sequence of each transcript using mRNA prepared from cells grown in XYS medium with 0.1 mM 4-HBA. The start site (C^{+1}) of the *pobA* transcript was identified at nucleotide −56 relative to the initiation codon ATG (Figure 2d), and a putative −35 element and −10 element sequence (TCGTCG-N_{21}-AATCAT) was assigned on the basis of conformity to the *E. coli* σ^{70}-promoter consensus sequence (Figure 2d). The role of the predicted −35 element of P_{pobA} in 4-HBA degradation was further verified by point mutation in the following section.

A 5′-RACE analysis identified a transcript start site (G^{+1}) within the promoter P_{pobR}. The latter start site is positioned 26 bp downstream of the predicted start codon ATG (Figure 2d). This occurrence is unusual since the transcription start site is normally located upstream of the start codon (Saecker *et al*., 2011). This result prompted us to re-annotate the *pobR* open reading frame (ORF) in XC1. A second putative start codon GTG was identified 69 bp downstream of the originally predicted start codon ATG (Figure 2d). To verify this new start codon, two ORFs from ATG or GTG to the stop codon TAA (named as *pobR* and $pobR^{GTG}$ respectively) were, respectively, amplified and cloned into the pBBR1MCS-2 vector. The resultant plasmids were transferred into strain Δ*pobR* to generate the strains Δ*pobR* (*pobR*) and Δ*pobR*($pobR^{GTG}$). In XOLN medium supplemented with 0.5 mM 4-HBA, the two strains displayed similar 4-HBA degradation capacities to that of wild-type strain XC1 (Figure 2b,c). These findings suggest that GTG could be the true start codon of PobR. Accordingly, the −10 and −35 elements (CGACGA-N_{17}-AATGTA) were assigned upstream of the defined transcriptional start site (G^{+1}) of *pobR* (Figure 2d). Notably, the −35 elements of P_{pobA} and P_{pobR} overlap completely in the intergenic region (Figure 2d).

2.4 | pobA transcription is specifically induced by 4-HBA via PobR

To monitor P_{pobA} activity, a DNA fragment spanning the 539 bp upstream of the start codon ATG of *pobA* was cloned into pMD18T-T0T1-*gusA*. The resultant P_{pobA}-*gusA* fusion was then integrated into the XC1 chromosome to generate the reporter strain XC1::P_{pobA}-*gusA* (Figure S3a). Using the constructed reporter strain XC1::P_{pobA}-*gusA*, *pobA* transcription levels were measured in the absence of 4-HBA during growth in XYS liquid medium. P_{pobA}-dependent β-glucuronidase (GUS) activities ranged from 1,127 unit/OD_{600} at 6 hpi to 1,418 unit/OD_{600} at 12 hpi, and then dropped to 453 unit/OD_{600} at 24 hpi and 171 unit/OD_{600} at 48 hpi (Figure 3a). In the XYS medium supplemented with 0.1 mM 4-HBA, P_{pobA}-dependent GUS activities ranged from 62,583 unit/OD_{600} at 6 hpi to 46,241 unit/OD_{600} at 12 hpi, and then dropped to 5,658 unit/OD_{600} at 24 hpi and 1817 unit/OD_{600} at 48 hpi (Figure 3a).

On the XYS agar plate supplemented with 50 μg mL^{-1} 5-bromo-4-chloro-3-indolyl-β-D-glucuronide (x-Gluc) (XYSG), the intensity of the blue color associated with colonies of the reporter strain XC1::P_{pobA}-*gusA* increased as the concentration of 4-HBA increased from 0.01 mM to 1.0 mM (Figures 3b and S3b). In the XC1::P_{pobA}-*gusA* cultures at 12 hpi, P_{pobA}-dependent GUS activities increased with 4-HBA concentration, ranging from 8,906 unit/OD_{600} at 0.01 mM to 36,285 unit/OD_{600} at 0.1 mM, and 174,641 unit/OD_{600} at 1.0 mM (Figure 3c).

Furthermore, as part of this analysis, we attempted to determine whether 4-HBA-like compounds exhibit similar stimulatory effects on *pobA* transcription. To this end, a total of nine compounds, 2-HBA; 3-HBA; 4-hydroxyphenylacetic acid (4-HPA); benzoic acid (BA); 2-aminobenzoic acid (2-ABA); protocatechuic acid (3,4-DHBA); methyl-4-hydroxybenzoate (M4HB); and butyl-4-hydroxybenzoate (B4HB), were individually added into the XYS cultures of the reporter strain XC1::P_{pobA}-*gusA* at a final concentration of 0.1–1.0 mM. Following analysis of GUS activities, we observed that none of these compounds promoted *pobA* transcription (Figure S4).

Finally, the fusion gene P_{pobA}-*gusA* was integrated into strain Δ*pobR* to generate the reporter strain Δ*pobR*::P_{pobA}-*gusA*. Following analysis

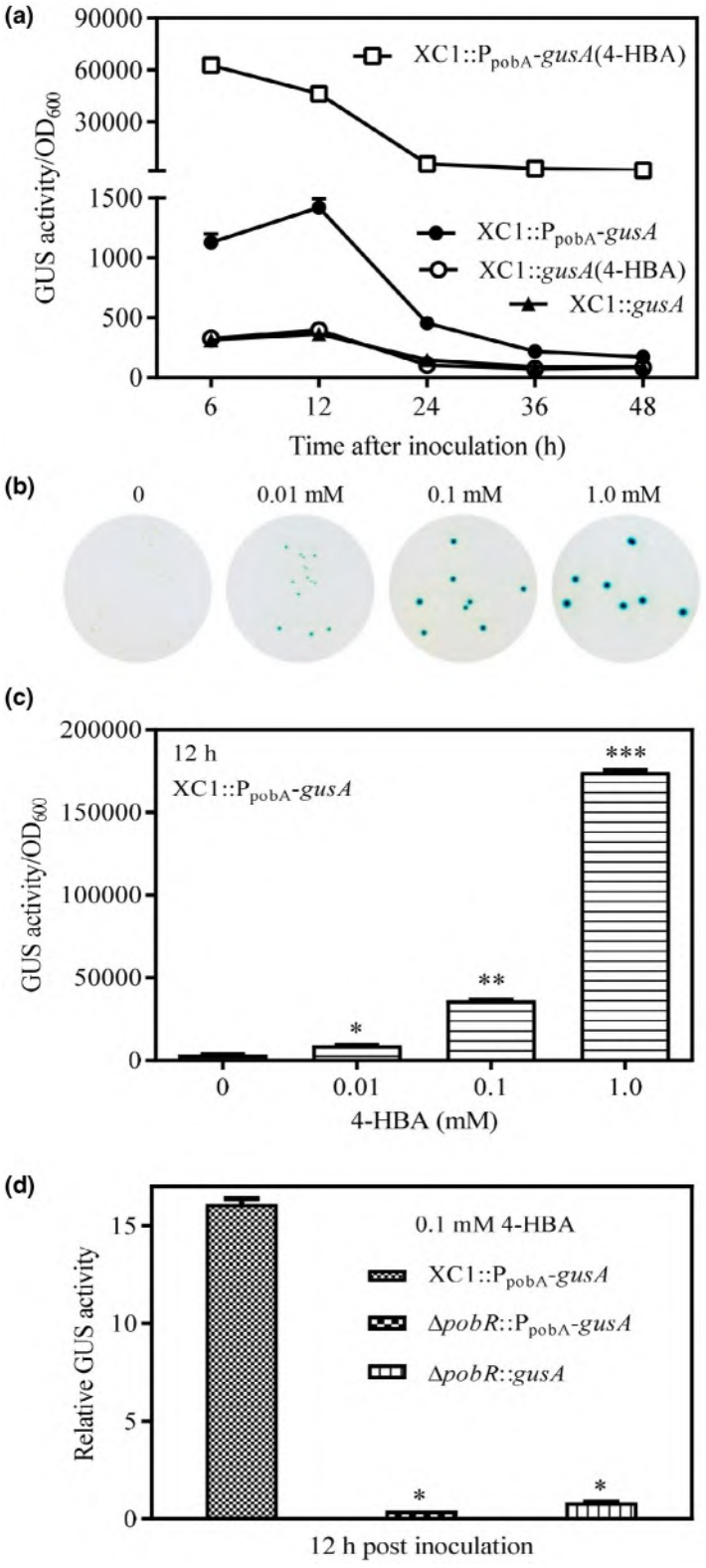

FIGURE 3 *pobA* transcription is specifically induced by 4-HBA via PobR. (a) Time course of P_{pobA}-dependent GUS activities in the absence and presence of 0.1 mM 4-HBA. (b) Colonies of XC1::P_{pobA}-*gusA* on XYS agar plate supplemented with 50 μg/mL x-Gluc and increasing concentrations of 4-HBA. (c) GUS activities of XC1::P_{pobA}-*gusA* cultures in the presence of 0.01-1.0 mM 4-HBA at 12 hpi. (d) The relative P_{pobA}-dependent GUS activities for strains XC1 and Δ*pobR* in the presence of 0.1 mM 4-HBA at 12 hpi. Shown are the averages for three technical repeats with standard deviation. Statistically significant differences are indicated by asterisks (one asterisk, $p \leq .05$; two asterisks, $p \leq .01$; three asterisks, $p \leq .001$) [Colour figure can be viewed at wileyonlinelibrary.com]

of GUS activities, we observed that the addition of 0.1 mM 4-HBA to the Δ*pobR*::P_{pobA}-*gusA* culture had little effect on *pobA* transcription (Figure 3d). Further qRT-PCR analysis also showed that *pobA* levels in the strains Δ*pobR*, Δ*pobRA* and Δ*pobRA*(*pobR*) are significantly lower than that in the wild-type strain XC1 (Figure S3c). These findings indicate that PobR is required for 4-HBA-induced *pobA* transcription.

2.5 | pobR is transcribed in the absence of 4-HBA, the presence of 4-HBA advances its expression

To monitor *pobR* transcription, the reporter strain XC1::P_{pobR}-*gusA* was generated using the method described in Figure S3a. Upon

growth in XYS liquid medium, P_{pobR}-dependent GUS activity in strain XC1::P_{pobR}-*gusA* ranged from 7,895 unit/OD_{600} at 6 hpi to 11,119 unit/OD_{600} at 12 hpi, then declining to 4,437 unit/OD_{600} at 24 hpi and 2,365 unit/OD_{600} at 48 hpi (Figure 4a). In accordance with the latter finding, the colonies of the reporter strain XC1::P_{pobR}-*gusA* were blue on the XYSG agar plate in the absence of 4-HBA (Figure 4b).

P_{pobR}-dependent GUS activity in strain XC1::P_{pobR}-*gusA* increased concomitantly with 4-HBA concentration on XYSG plates or in XYS liquid cultures (Figure 4b,c). The addition of 0.1 mM 4-HBA to XYS liquid cultures significantly increased XC1::P_{pobR}-*gusA* culture GUS activity by 75% (at 6 hpi), 66% (at 12 hpi) and 145% (at 24 hpi) respectively (Figure 4a).

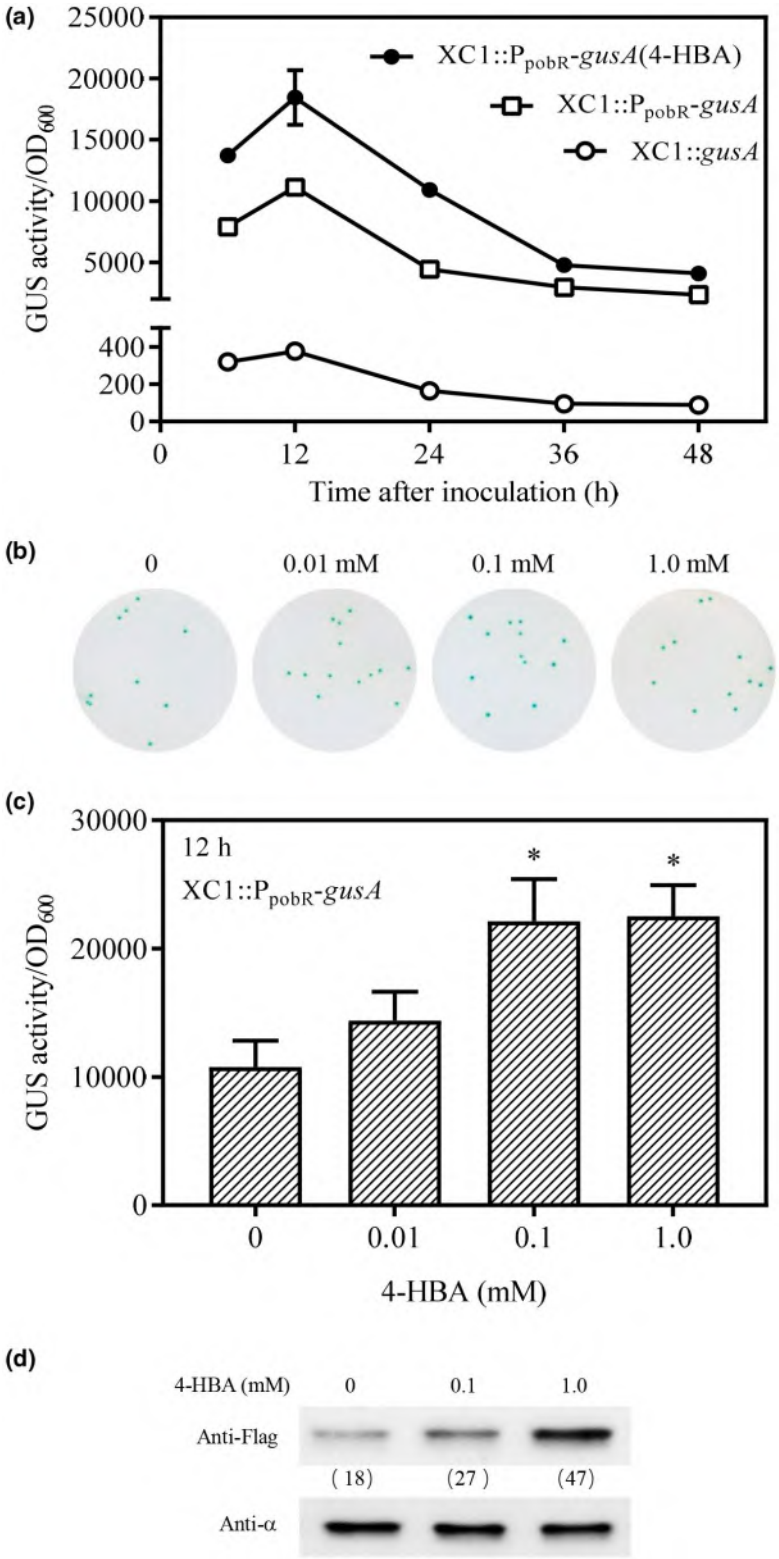

FIGURE 4 *pobR* expression pattern during growth. (a) Time course of P_{pobR}-dependent GUS activities in the absence and presence of 0.1 mM 4-HBA. (b) Colonies of XC1::P_{pobR}-*gusA* on XYS agar plate supplemented with 50 μg/mL x-Gluc and increasing concentrations of 4-HBA. (c) P_{pobR}-dependent GUS activities in the presence of 0.01 mM to 1.0 mM 4-HBA at 12 hpi. (d) Western blotting analysis showing PobR protein levels in the presence of 0.1 mM and 1.0 mM 4-HBA. (Upper) Western blot probed with an antibody against Flag tag; (Lower) Western blot probed with an antibody against the α subunit of RNA polymerase, which was used as a control for sample loading. The numbers indicate signal intensity as measured using ImageJ software (http://rsb.info.nih.gov/ij/). Shown are the averages for three technical repeats with standard deviation. Statistically significant differences are indicated by one asterisk ($p \leq .05$) [Colour figure can be viewed at wileyonlinelibrary.com]

To further verify the effects of 4-HBA on *pobR* transcription, we analyzed PobR protein levels via Western blotting. To this end, two Flag coding sequences were fused into *pobR* in the XC1 chromosome. The resultant strain XC1::*pobR*-flag$_2$ exhibited similar 4-HBA degradation activity as XC1 strain (Figure S5a), suggesting that the fused Flag sequences do not affect PobR functionality in vivo. Thus, the commercially available monoclonal antibody against Flag was used to detect the PobR-Flag$_2$ fusion protein. The results revealed that the addition of 0.1 mM and 1.0 mM 4-HBA increased PobR protein levels by 50.0% and 162.5% respectively (Figure 4d).

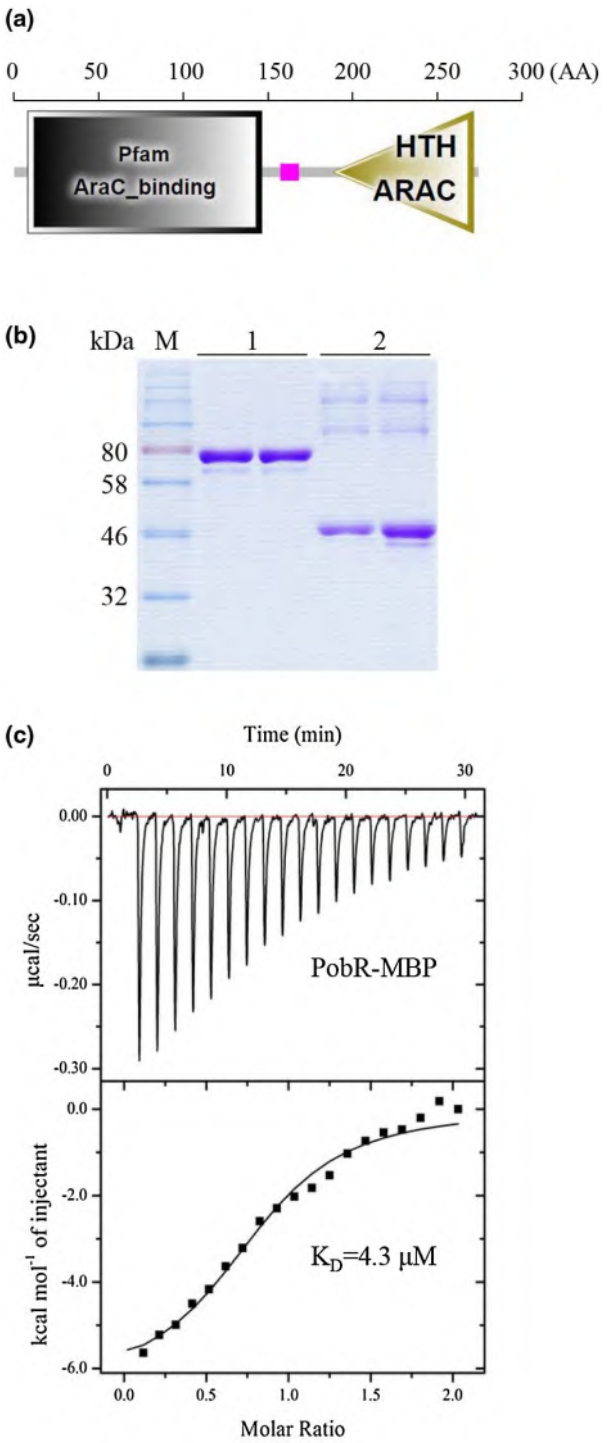

FIGURE 5 PobR directly binds 4-HBA. (a) Domain structure of PobR as predicted by SMART (http://smart.embl-heidelberg.de). (b) SDS–PAGE analysis of purified PobR-MBP fusion protein and MBP protein. 1: purified PobR-MBP fusion protein; 2: purified MBP protein. (c) Isothermal titration calorimetry analysis of the binding of 4-HBA to PobR-MBP [Colour figure can be viewed at wileyonlinelibrary.com]

2.6 | PobR specifically binds 4-HBA

pobR encodes a 274-amino acid transcriptional factor with a N-terminal AraC-type effector binding domain and a C-terminal helix-turn-helix (HTH) DNA binding domain (Figures 5a and S6). Heterologous expression of the full-length *pobR* gene in *E. coli* BL21 (DE3) strain failed to yield soluble protein; however, heterologous expression of the *pobR* and maltose-binding protein (*mbp*) fusion gene *pobR-mbp* yielded soluble PobR-MBP fusion protein. Overexpression of either the *pobR-mbp* fusion gene or *pobR* alone complemented strain Δ*pobR* in relation to 4-HBA degradation ability (Figure S5b), suggesting that the MBP tag does not affect PobR functionality in vivo. The MBP-tagged PobR fusion protein was purified using maltose affinity chromatography (Figure 5b). Size exclusion chromatography (SEC) analysis suggested that all the purified PobR-MBP fusion proteins in buffer A were decamers (Figure S7a-c). In buffer B, 76.6% of the purified PobR-MBP fusion proteins were dimers (Figure S7d). In contrast, MBP proteins were monomers in both buffers A and B (Figure S7e).

As shown in Figure 5c, isothermal titration calorimetry (ITC) analysis showed that 4-HBA directly binds PobR-MBP dimer proteins at a 1:1 molar ratio and with a dissociation constant (K_d) of 4.3 μM. Conversely, no binding was detected between 4-HBA and the MBP tags (Figure S8a). Furthermore, no binding was observed between PobR-MBP and the 4-HBA analogues, 2-HBA and 3-HBA (Figure S8b,c). The PobR-MBP decamers and the XC1-specific RpfF protein did not exhibit 4-HBA-binding activity (Figure S8d,e).

2.7 | Key residues required for 4-HBA binding and dimerization in PobR

To better understand the mechanisms underpinning the binding of 4-HBA to PobR and subsequent dimerization, a multiple sequence alignment analysis of *Xcc* PobR and other AraC family members of PobR was performed. The analysis identified a range of conserved amino acid residues at the N-terminal ligand binding region of PobR (Figure S9). To verify the roles of these residues in the binding of 4-HBA to PobR and/or PobR dimerization, the nine conserved residues, that is, H^8, R^{15}, H^{19}, W^{21}, R^{27}, Q^{33}, Y^{36}, H^{67} and R^{134}, were individually mutated into D^8, E^{15}, D^{19}, G^{21}, E^{27}, L^{33}, L^{36}, D^{67} and E^{134}, respectively, in PobR-MBP (Table 1). The mutated proteins, PobR-HD^8, PobR-RE^{15}, PobR-HD^{19}, PobR-WG^{21}, PobR-RE^{27}, PobR-QL^{33}, PobR-YL^{36}, PobR-HD^{67} and PobR-RE^{134} were, respectively, dissolved in buffer B at a final concentration of 5 mg mL^{-1}.

SEC analysis revealed that 71.9%, 77.2% and 66.3% of PobR-HD^{19}, PobR-WG^{21} and PobR-QL^{33} remained as dimers in buffer B, respectively (Table 1 and Figure S10); this result suggests that H^{19}, W^{21} and Q^{33} are not required for dimerization. In contrast, 49.6% and 41.3% of PobR-RE^{15} and PobR-YL^{36} remained as dimers in buffer B, respectively; PobR-HD^{8}, PobR-RE^{27}, PobR-HD^{67} and PobR-RE^{134} were almost all decamers in buffer B (Table 1 and Figure S10a,b).

The dimers of PobR-RE^{15}, PobR-HD^{19}, PobR-GW^{21}, PobR-QL^{33} and PobR-YL^{36} were collected by SEC and adjusted to a final concentration of 50 μM. ITC analysis was conducted to detect the binding of 4-HBA to these dimers. The Kd values for the dimers PobR-RE^{15}, PobR-WG^{21} and PobR-YL^{36} were 22.3 ± 1.6, 11.5 ± 1.8 and 9.5 ± 1.3, respectively; these values are significantly higher than that for PobR (4.3 ± 0.8) (Table 1 and Figure S11). The mutated PobR dimers, PobR-HD^{19} and PobR-QL^{33}, had no 4-HBA binding ability (Table 1 and Figure S11). Furthermore, to verify the roles of the nine residues in 4-HBA degradation, point mutations were independently and separately introduced to the *pobR* gene in the *Xcc* chromosome. The resultant mutation strains, XC1::HD^{8}, XC1::RE^{15}, XC1::HD^{19}, XC1::WG^{21}, XC1::RE^{27}, XC1::QL^{33}, XC1::YL^{36}, XC1::HD^{67} and XC1::RE^{134}, were analyzed for 4-HBA degradation ability (Table 1). The results showed that mutation of R^{15}, H^{19}, R^{27}, Q^{33} and H^{67} abolished 4-HBA degradation ability; mutation of H^{8}, W^{21}, Y^{36} or R^{134} significantly reduced 4-HBA degradation ability (Figure S12 and Table 1).

2.8 | PobR specifically binds to a 25-bp site within the overlapping promoters

The DNA-binding activities of PobR were first examined using electrophoretic mobility shift assays (EMSA). The specific DNA probe, a 233-bp DNA fragment corresponding to the intergenic region between the ORFs of *pobA* and *pobR*, was amplified by PCR using a pair of Cy5-labeled primers (Table S3). In the absence of 4-HBA, high levels of PobR-MBP dimers could bind the Cy5-labeled probe (Cy5-P_A) to form two types of shifts. Shift 1 was the dominant one observed in the presence of 0.1-0.4 μM PobR-MBP dimers; Shift 2 was the dominant one in the presence of 1.6-3.2 μM PobR-MBP dimers (Figure 6a). In contrast, the MBP protein did not cause a shift of the Cy5-P_A (Figure 6a).

In the presence of 4-HBA, Shift 1 was observed even in the presence of low levels of PobR-MBP dimers (0.05 μM). The addition of increasing concentrations of 4-HBA significantly increased the formation of band Shift 1 (Figure 6b). No significant binding was detected between the Cy5-P_A and PobR-MBP decamers at 0.2 μM to 0.8 μM; PobR-MBP decamers at higher levels (1.6 μM to 6.4 μM) exhibited weak binding activity to the Cy5-P_A (Figure S13a). The XC1-specific protein RpfF had no binding to the Cy5-P_A probe (Figure S13b).

To identify the precise PobR binding site, DNase I footprinting analysis was performed using the purified PobR-MBP dimers and the 233-bp intergenic region as the DNA probe. A representative sequencing result is shown in Figure 6c. The data show that PobR can protect a 25-bp DNA region "GTGGGCATCGTCGAAAAGTCCAAGC" from DNase I digestion. An alignment of the intergenic sequences from seven *Xanthomonas* genomes revealed the presence of conserved residues in the PobR operator site (Figure 7a). This PobR-protected site fully covers the overlapping −35 elements of both P_{pobA} and P_{pobR} (Figures 2d and 7a).

Further analysis revealed that the 25-bp PobR binding site contains an imperfect inverted repeat sequence indicated by the red and blue arrows in Figure 7a. To understand the detailed interaction, the 25-bp region was further divided into three sub-regions: P_I, P_{II} and P_{III} (Figure 7a). GTGG of P_I, TCGT of P_{II} and GTCC of P_{III} were, respectively, mutated into AAAA to generate three variants, $P_{I(A)}$, $P_{II(A)}$ and $P_{III(A)}$. The three variants were subjected to promoter activity assays and EMSA analysis for PobR binding ability. Results of a GUS activity analysis revealed that mutation of P_I had little effect on the 4-HBA-induced P_{pobA} activity, whereas mutation of P_{II} or P_{III} completely abolished the 4-HBA-induced P_{pobA} activity (Figure 7b). EMSA analysis showed that variant probe $P_{I(A)}$ was still able to bind to the PobR dimers to form Shift 1, whereas variant $P_{II(A)}$ or $P_{III(A)}$ was unable to bind to PobR (Figure 7c).

TABLE 1 The roles of nine residues on dimerization and 4-HBA binding activity in PobR

Mutation	Dimerization	4-HBA binding (Kd) (μM)	4-HBA degradation ratio (%) at 18 hpi
PobR	76.6 ± 0.9%	4.3 ± 0.8	100
PobR-HD^{8}	5.9 ± 0.8%^{a}	no binding (decamer)	80.0 ± 3.7^{a}
PobR-RE^{15}	49.6 ± 0.7%^{b}	22.3 ± 1.6^{a}	0
PobR-HD^{19}	71.9 ± 0.8%	no binding	0
PobR-WG^{21}	77.2 ± 0.8%	11.5 ± 1.8^{a}	48.6 ± 2.9^{b}
PobR-RE^{27}	0.0	no binding (decamer)	0
PobR-QL^{33}	66.3 ± 0.9%	no binding	0
PobR-YL^{36}	41.3 ± 0.7%^{b}	9.5 ± 1.3^{b}	94.0 ± 5.5
PobR-HD^{67}	0.0	no binding (decamer)	0
PobR-RE^{134}	0.0	no binding (decamer)	56.0 ± 4.7^{b}

Note: The statistically significant differences ($p \leq 0.05$) are indicated by different letter a or b.

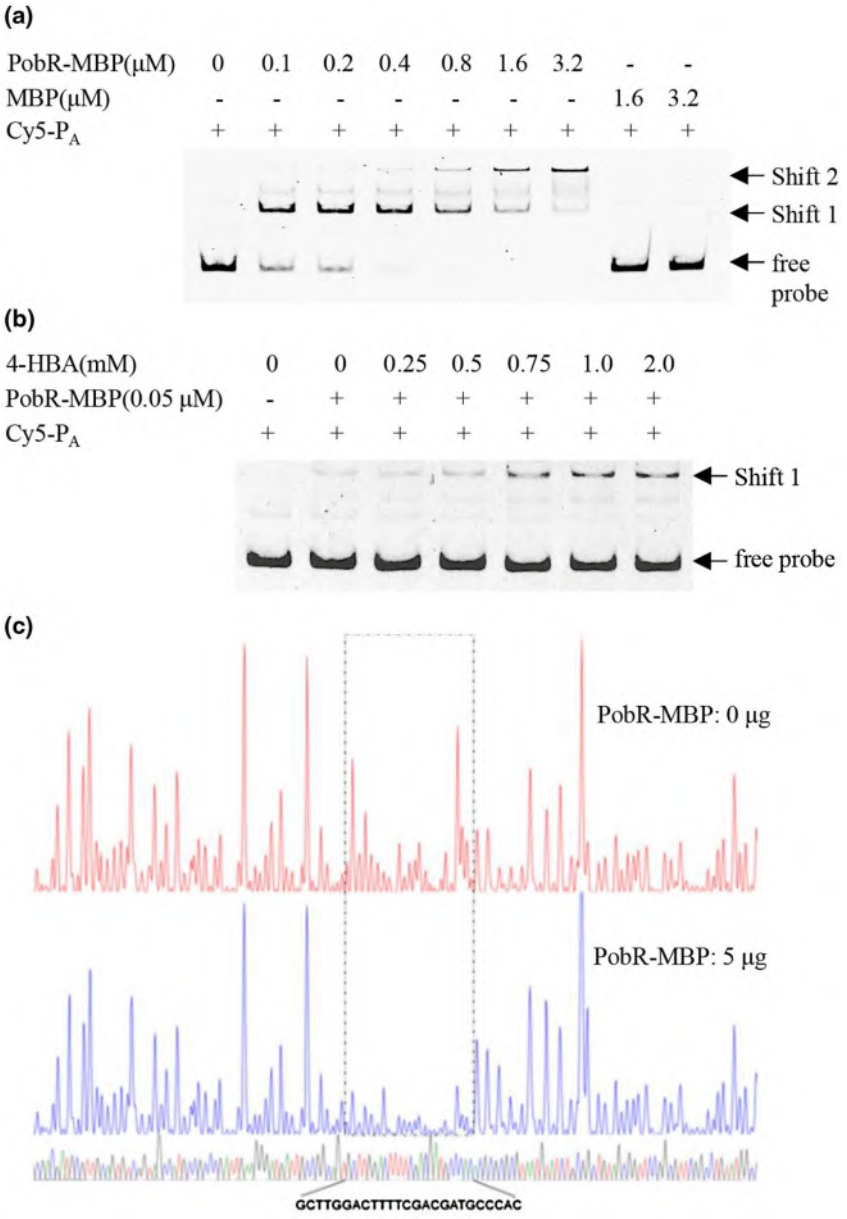

FIGURE 6 PobR specifically binds to a 25-bp site in the intergenic region of *pobR* and *pobA*. (a) EMSA was performed using a 233-bp Cy5-labeled probe P_A (Cy5-P_A) and 0.1 μM to 3.2 μM PobR-MBP. (b) EMSA was performed using Cy5-P_A and 0.05 μM PobR-MBP in the presence of 0.25 mM to 2 mM 4-HBA. (c) DNase I footprinting sequencing was performed using purified PobR-MBP and a 233-bp fluorescent FAM-labeled DNA probe P_A [Colour figure can be viewed at wileyonlinelibrary.com]

The same point mutations were introduced into P_I, P_{II} or P_{III} in the XC1 chromosome. The resultant mutant strains, XC1::$P_{I(A)}$, XC1::$P_{II(A)}$ and XC1::$P_{III(A)}$, were examined for 4-HBA degradation ability. The results revealed that the 4-HBA degradation ability of strains XC1::$P_{II(A)}$ and XC1::$P_{III(A)}$ was lost (Figure 7d), suggesting that P_{II} and P_{III} in the 25-bp region are important for PobR binding.

2.9 | Both pobR and pobA are transcribed during XC1 infection inside Chinese radish

So far, all data pertaining to the transcriptional induction of *pobR* and *pobA* have been based on in vitro cell culturing. *Xcc* is a xylem-dwelling phytopathogen and the conditions for *Xcc in planta* growth are probably different from those required for in vitro culturing. To elucidate the roles of the 4-HBA degradation system in *Xcc* infection, we believe it is important to determine if the 4-HBA degradation genes are expressed after *Xcc* infects the host plants. To this end, the XC1 strains carrying the *pobA* and *pobR* reporter gene constructs, XC1::P_{pobA}-*gusA* and XC1::P_{pobR}-*gusA*, respectively, were introduced into Chinese radish by the scissor clipping method.

Histochemical staining analysis detected P_{pobR}- and P_{pobA}-dependent GUS expression inside the infected leaf tissues (Figure 8a). No significant difference in cell numbers was observed among all the infected leaves that were analyzed at 3- and 5-days post inoculation (Figure 8a). Subsequent GUS quantitative assay demonstrated that the expression level of *pobR* is slightly higher than that of *pobA* in XC1 inside the infected tissues. However, the expression levels of both *pobA* and *pobR* are lower than that of *hrpX*, a regulator gene for the type III secretion system (Figure 8a,b).

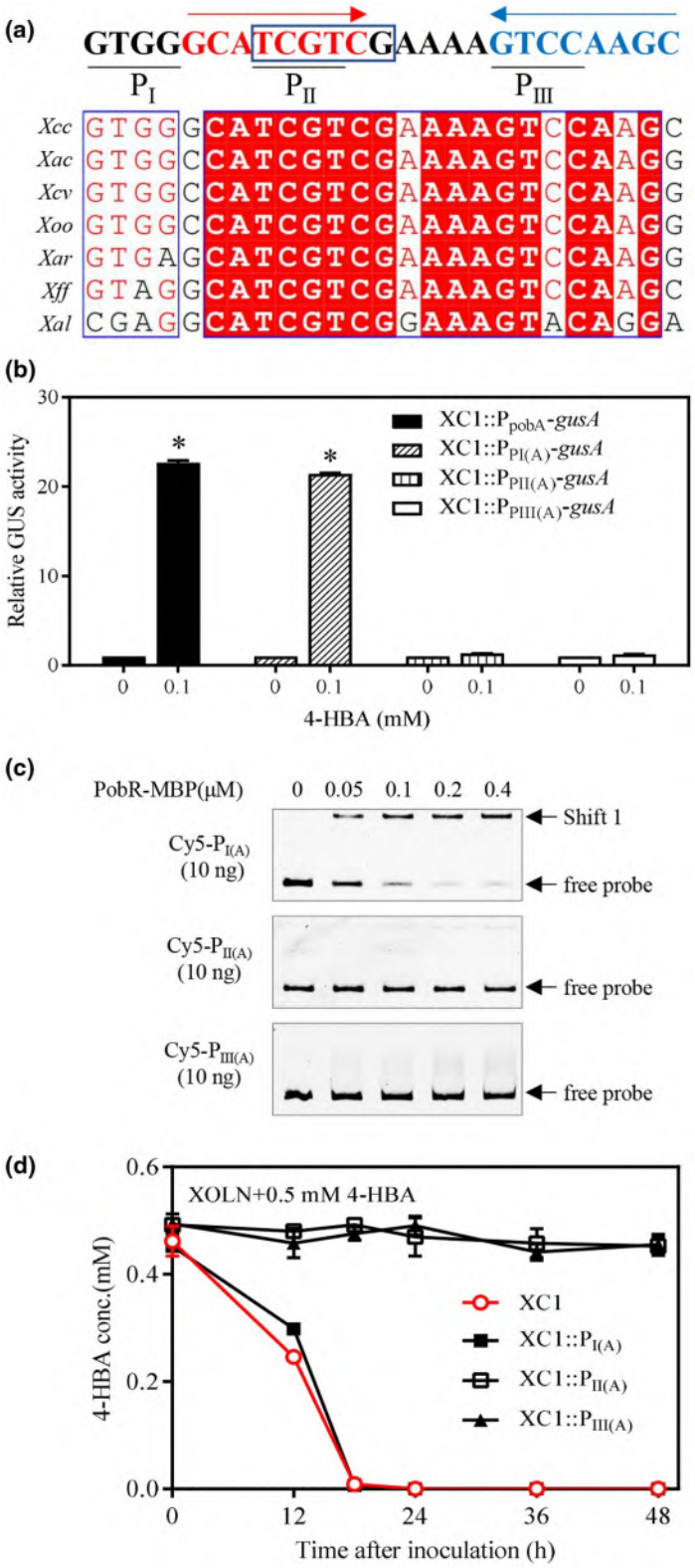

FIGURE 7 Further verification of the PobR-binding site. (a) The three subregions, the overlapping −35 elements (in the rectangular box) and the putative inverted repeat sequences within the 25-bp binding site. (b) The relative GUS activities of the XC1 strains driven by the mutated *pobA* promoters $P_{I(A)}$, $P_{II(A)}$ or $P_{III(A)}$ in the presence and absence of 0.1 mM 4-HBA. (c) EMSA analysis of the binding between PobR-MBP and the mutated Cy5-labeled probes $P_{I(A)}$, $P_{II(A)}$ and $P_{III(A)}$. (d) 4-HBA degradation activities of the XC1 strains with point mutation in the three subregions P_I, P_{II} and P_{III}. Shown are the averages for three technical repeats with standard deviation. Statistically significant differences are indicated by one asterisk ($p \leq .05$) [Colour figure can be viewed at wileyonlinelibrary.com]

2.10 | pobR is required for full pathogenicity of XC1 in Chinese radish and cabbage

A previous study reported that the Δ*pobA* strain displayed compromised virulence in Chinese radish (Wang *et al*., 2015). In this study, the *pobR* mutant and the complementation strain Δ*pobR*::*pobR* were further analyzed for virulence in Chinese radish and cabbage using the leaf-clipping method. The results revealed that the average lesion length of strain Δ*pobR* in Chinese radish is 12.8 mm, which is significantly shorter than those of strains XC1 (16.4 mm) and Δ*pobR*::*pobR* (15.6 mm) 2 weeks post inoculation (Figure 8c). Similarly, the average lesion length of strain Δ*pobR* is 10.0 mm in cabbage, which is significantly shorter than those of strains XC1 (16.6 mm) and Δ*pobR*::*pobR* (15.3 mm) 2 weeks post inoculation (Figure 8c).

3 | DISCUSSION

The present study demonstrated that *Xcc*-infected host plants produce more 4-HBA to combat the pathogen, and *Xcc* can efficiently degrade 4-HBA via the *pobA*/*pobR* locus to overcome the stress. Both *pobA* and *pobR* genes are divergently transcribed, but share completely overlapping −35 elements in their promoter regions.

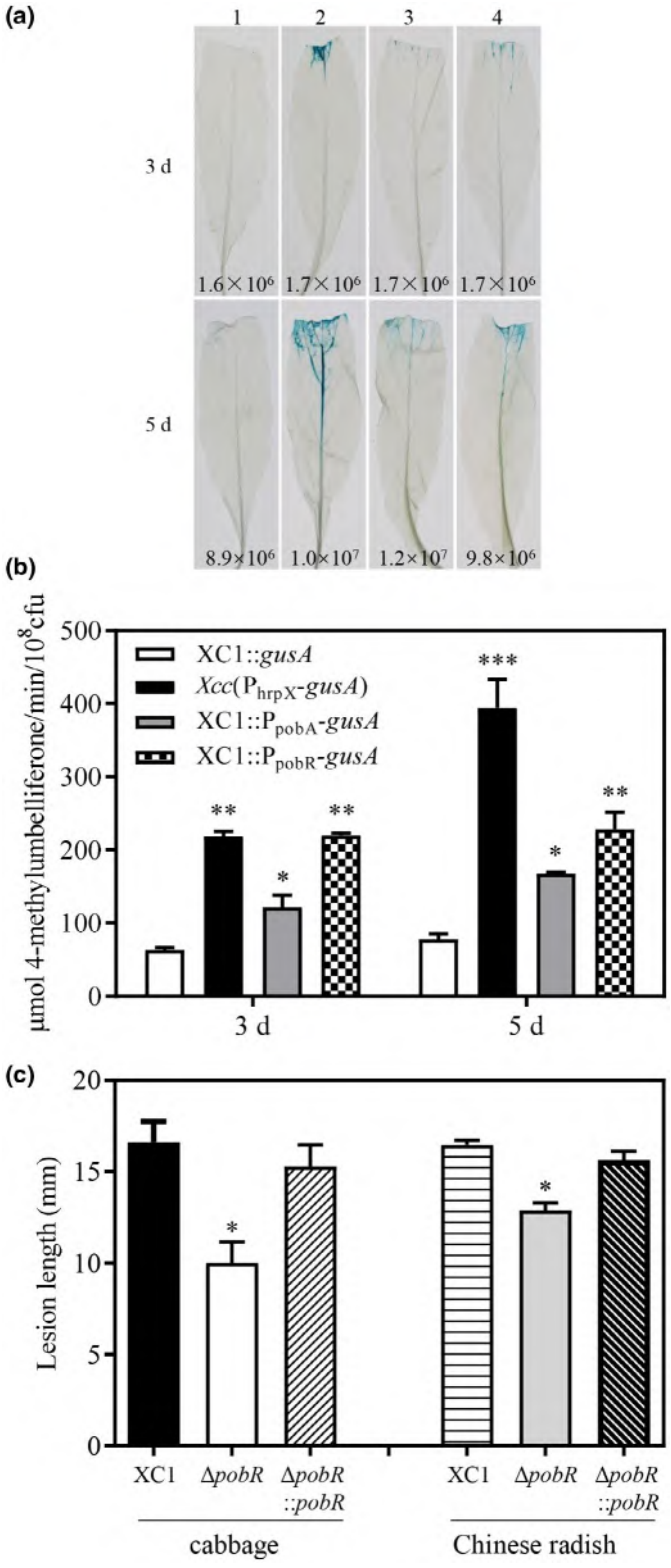

FIGURE 8 The *pobR*/*pobA* locus is contributing to XC1 virulence in cabbage and Chinese radish. (a) Bacterial colony formation units (CFU) and GUS histochemical staining in infected Chinese radish leaves at 3- and 5-days post inoculation. (1): XC1::*gusA*; (2): *Xcc*(P_{hrpX}-*gusA*); (3): XC1::P_{pobA}-*gusA*; (4): XC1::P_{pobR}-*gusA*. (b) Quantitative analysis of different promoter-driven GUS activities per 10^8 CFU of the *Xcc* strains inside Chinese radish using 4-methylumbelliferyl-β-D-glucuronide as a substrate at 3- and 5-days post inoculation. (C) The lesion length of strains XC1, Δ*pobR* and Δ*pobR*::*pobR* two weeks after inoculation in cabbage and Chinese radish. Statistically significant differences are indicated by asterisks (one asterisk, $p \leq 0.05$; two asterisks, $p \leq .01$; three asterisks, $p \leq .001$) [Colour figure can be viewed at wileyonlinelibrary.com]

4-HBA specifically binds to PobR dimer at 1:1 ratio to form 4-HBA/PobR dimer complex, which further binds to a 25-bp site within the overlapping promoters to activate *pobR* and *pobA* transcription. Both genes are transcribed during *Xcc* infection of Chinese radish and are required for full pathogenicity in host plants. These findings suggest that *Xcc* utilizes the PobA/PobR-dependent 4-HBA degradation system to evade or subvert phenolic compound stress to facilitate the successful colonization of host plants.

3.1 | Biochemical basis for 4-HBA recognition and PobR dimerization

PobR homologs are generally categorized into two major functional groups (Tropel and van der Meer, 2004). The AraC family of PobR proteins are characterized by a C-terminal 100-residue stretch containing an AraC-type helix-turn-helix DNA binding domain (Figure S6). The IclR family of PobR proteins are characterized by an N-terminal HTH DNA binding domain and a C-terminal IclR-type ligand binding domain (Figure S6). None of these PobR homologues apart from the unusual *Streptomyces* PobR were purified in a soluble format (Zhang *et al*., 2018). This lack of solubility hampers our understanding of the molecular mechanisms that underpin 4-HBA degradation. The results obtained in this study support the usefulness of PobR-MBP fusion protein as a replacement for PobR to study the molecular interactions between PobR, 4-HBA and target promoter.

An understanding of how PobR binds 4-HBA via its ligand binding domain is crucial for the elucidation of PobR regulation during 4-HBA catabolism. In *Acinetobacter* strain ADP1, the IclR family of PobR was shown to be dependent on 4-HBA for its activity; this dependence was only diminished following the substitution of four amino acids (S^{118}, E^{124}, E^{126} and L^{138}) in the central region of the protein (Kok *et al*., 1998). Crystal structure analysis of the PobR/4-HBA complex in *S. coelicolor* showed that the N-terminal IclR ligand binding domain is the only region of the protein capable of facilitating binding to 4-HBA (Zhang *et al*., 2018). The hydroxyl group of 4-HBA is involved in salt bridge and hydrogen bonding interactions with side chains of Gln^{125}, Arg^{130} and Asp^{208} and with the backbone amide of Ala^{148}. The 4-HBA aromatic moiety also exhibits hydrophobic interactions with Phe^{122}, Phe^{136}, Ala^{218} and Val^{238} (Zhang *et al*., 2018). Multiple

sequence alignment analysis revealed that the putative 4-HBA interacting residues in the IclR family of PobR in *Acinetobacter* strain ADP1 and *S. coelicolor* are not conserved in *Xcc* PobR (Figure S9). Instead, the AraC family members of PobR contain a range of conserved residues in the ligand-binding region (Figure S9). The present study revealed that only the PobR dimer exhibits 4-HBA binding activity. The combination of SEC analysis, ITC assay and 4-HBA degradation ability suggest that five residues, R^{15}, H^{19}, W^{21}, R^{27}, Q^{33} and H^{67}, are likely to be involved in 4-HBA binding (Table 1 and Figures S10-S12). Interestingly, these residues are not conserved in the IclR family of PobR in *Acinetobacter* strain ADP1 and *S. coelicolor*, suggesting that an alternative mechanism for 4-HBA recognition and subsequent activation of *pobA* expression might be used by AraC-type PobR. This hypothesis is further supported by the finding that the direct binding of 4-HBA destabilizes binding between PobR and its target DNA in *S. coelicolor* (Zhang *et al*., 2018) whereas the addition of increasing concentrations of 4-HBA significantly increased the formation of the PobR/DNA probe complex in this study (Figure 6b). Further crystal characterization of the PobR-4HBA complex will provide further insights into the interactions among 4-HBA, PobR and P_{pobA}.

Dimerization facilitates the insertion of HTH domains onto the inverted repeat sequences of targeting promoters; this occurrence is believed to further enhance DNA-binding specificity (Ni *et al*., 2013). As part of this study, two different conformations were observed for *Xcc* PobR; dimers in buffer B and decamers in buffer A (Figure S7a–d). The decamer conformation is uncommon and is probably due to in vitro protein aggregation of monomers at high concentrations. Inside *Xcc* cells, PobR most likely exists as either a monomer or dimer. This is consistent with the finding that the unusual PobR found in *Streptomyces* is a dimer in the absence of 4-HBA and a monomer in the presence of 4-HBA (Zhang *et al*., 2018). The present study further revealed that residues, H^{8}, R^{15}, R^{27}, Y^{36}, H^{67} and R^{134}, are most likely involved in in vitro dimerization (Table 1 and Figure S10). All the latter residues are fully or partially required for *Xcc* 4-HBA degradation ability (Figure S12 and Table 1). Interestingly, three of these residues, R^{15}, R^{27} and H^{67}, were also shown to be required for 4-HBA binding (Table 1 and Figure S11), thus confirming that 4-HBA binding is associated with PobR dimerization.

3.2 | Roles of overlapping promoters in PobR-dependent pobA transcription

In almost all the reported 4-HBA-degrading bacterial species including *Xcc*, *pobA*/*pobR* systems generally exhibit tight genetic organization, with overlapping promoters for the divergently transcribed genes *pobA* and *pobR* (Dimarco and Ornston, 1994) (Figure 2a). However, very little is known about promoter organization and the roles of the overlapping promoters in PobR-dependent *pobA* transcription. In the present study, we performed a detailed bioinformatics and genetic analysis of the overlapping promoters. The transcription start sites of *pobA* and *pobR* were identified by 5′-RACE; the *pobR* ORF was experimentally re-annotated and the −10 elements and −35 elements of both genes were defined (Figure 2d). Surprisingly, P_{pobA} and P_{pobR} share completely overlapping −35 elements. The PobR binding site fully encompasses the shared −35 elements of P_{pobA} and P_{pobR} (Figure 2d). To the best of our knowledge, this phenomenon has never been previously reported. Maintenance of this unique structure likely results in a highly effective and precise regulatory mechanism: PobR and RNA polymerase complex binding simultaneously controls both *pobA* and *pobR* transcription through superimposition of the −10 elements and −35 elements.

Analysis of the overlapping promoters also give a clue why *pobA* is not active, whereas *pobR* is active in the absence of 4-HBA (Figures 3 and 4). The − 10 and − 35 elements together constitute the classical prokaryotic promoter (Browning and Busby, 2016). The optimum space between the − 10 and − 35 elements of an active gene is 17 ± 1 bp (Saecker *et al*., 2011; Su *et al*., 2016). Consistent with this finding, the space between the − 10 and − 35 elements (CGACGA-N_{17}-AATGTA) of P_{pobR} is 17 bp, and *pobR* is active in the absence of 4-HBA (Figures 2d and 4). In contrast, the space between the − 35 and − 10 elements of P_{pobA} is 21 bp (Figure 2d). Su *et al*. (2016) showed that mutant promoters with a 19-bp-spacer in the *gumB* promoter generated limited amounts of transcripts, while the wild type (with a 16-bp-spacer) and the mutant promoters with either a 17- or 18-bp-spacer produced large amounts of transcript in *Xcc*. It has been proposed that additional transcriptional factors are required to bind to the long spacer sequences (Browning and Busby, 2004). The binding reaction either twists or bends the DNA to re-orientate the − 10 and − 35 elements so that they can be bound by the RNAP complex. Currently, the role of the 21-bp spacer sequence in P_{pobA} activity is being analyzed through point mutation and structural analyses of the PobR/promoter complex.

3.3 | A working model for 4-HBA/PobR-dependent pobA transcription during Xcc infection inside host plants

Upon analysis of these data, we propose a working model to describe how *Xcc* recognizes 4-HBA and induces *pobA* expression in vitro or *in planta* (Figure 9). When grown in culture with limited 4-HBA or at the epiphytic growth stage on the surface of host plants, intracellular 4-HBA levels fall below the threshold level and 4-HBA does not bind to PobR. PobR proteins exist as monomers and do not bind to the overlapping promoters P_{pobA} and P_{pobR}. RNA polymerase complex binds at the overlapping promoters, covering the full P_{pobR} (including −10 and −35 elements) and the partial P_{pobA} (−35 element only). It is likely that this binding pattern is sufficient to initiate *pobR* transcription, but not sufficient for *pobA* transcription. Thus, *pobR* is transcribed and constitutively active whereas *pobA* is not transcribed (Figure 9a).

In the presence of 4-HBA or at the *in planta* stage inside host plants, intracellular 4-HBA levels are above the threshold level and 4-HBA binds to PobR. The resultant 4-HBA/PobR dimer complex binds the 25-bp site within the overlapping promoters of P_{pobA} and

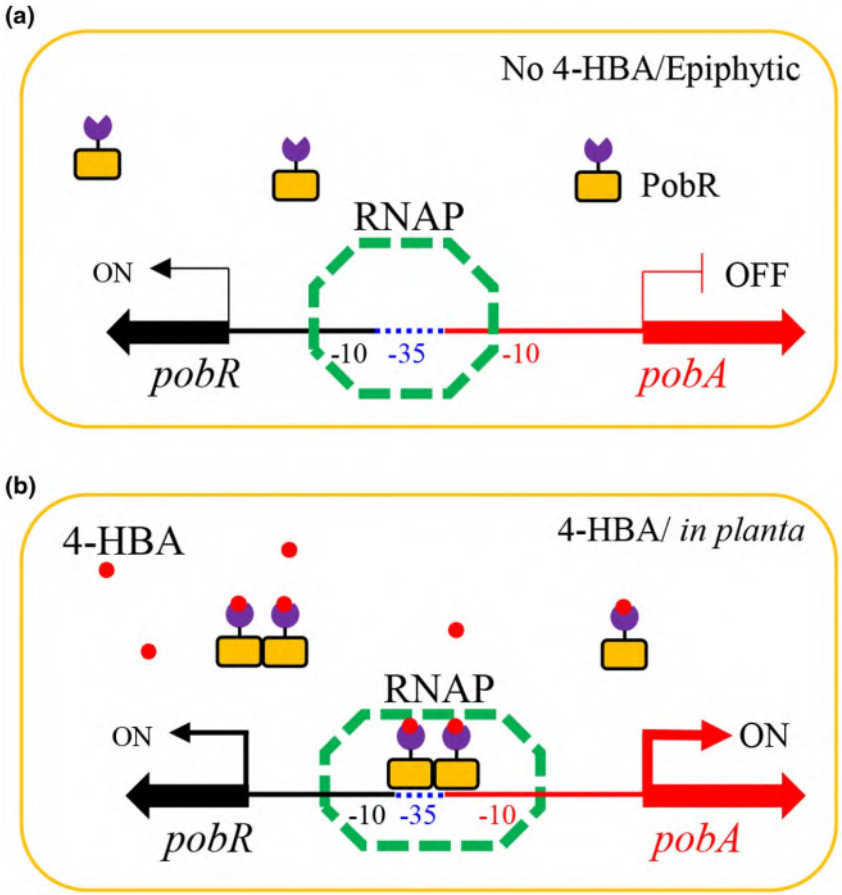

FIGURE 9 Schematic model for 4-HBA-dependent *pobA* transcription in *Xcc*. (a) When *Xcc* is grown in culture with limited 4-HBA or at the epiphytic growth stage on the surface of host plants, the intracellular 4-HBA levels in *Xcc* are below the threshold level, and 4-HBA does not bind to PobR. PobR proteins exist as monomers and do not bind to the overlapping promoters P_{pobA} and P_{pobR}. RNA polymerase complex binds at the overlapping promoters, covering the full P_{pobR} (including −10 and −35 elements) and part of P_{pobA} (−35 element only). Thus, *pobR* is transcribed and constitutively active whereas *pobA* is not transcribed. (b) In the presence of 4-HBA or during the *in planta* stage inside host plants, the intracellular 4-HBA in *Xcc* is above the threshold level, and 4-HBA binds to PobR. The resulting 4-HBA/PobR dimer complex binds into the 25-bp site within the overlapping promoters of P_{pobA} and P_{pobR}. The −10 and −35 elements of both P_{pobA} and P_{pobR} are bound by the RNA polymerase/PobR complex. This initiates *pobA* transcription and further increases *pobR* expression [Colour figure can be viewed at wileyonlinelibrary.com]

P_{pobR}. PobR binding most likely spans the region encompassing the overlapping promoters bound by the RNA polymerase complex. All the −10 and −35 elements of both P_{pobA} and P_{pobR} are bound by the RNA polymerase/PobR complex. The latter binding reaction, in turn, initiates *pobA* transcription and further increases *pobR* expression (Figure 9b).

4 | EXPERIMENTAL PROCEDURES

4.1 | Bacterial strains and culture conditions

The bacterial strains and plasmids used in the present study are listed in Tables S1 and S2. In most of the experiments performed during this study, *Xcc* wild-type strain XC1 and its derivatives were grown at 28°C in XOLN medium (0.7 g L^{-1} K_2HPO_4, 0.2 g L^{-1} KH_2PO_4, 1 g L^{-1} $(NH_4)_2SO_4$, 0.1 g L^{-1} $MgCl_2.6H_2O$, 0.01g L^{-1} $FeSO_4.7H_2O$, 0.001 g L^{-1} $MnCl_2.4H_2O$, 0.0625% yeast extract, 0.0625% tryptone, pH 7.15) or XYS medium (XOLN medium supplemented with 5 g L^{-1} sucrose). *E. coli* strains were grown at 37°C in LB medium (10 g L^{-1} tryptone, 5 g L^{-1} yeast extract, 20 g L^{-1} NaCl, pH 7.0). The antibiotics were added at the following concentrations when required: rifampicin (Rif) 25 μg mL^{-1}, kanamycin (Km) 50 μg mL^{-1}, gentamicin (Gm) 20 μg mL^{-1} and ampicillin (Amp) 100 μg mL^{-1}. Bacterial growth was determined by measuring optical density at a wavelength of 600 nm.

4.2 | Gene deletion and functional complementation analysis

The *Xcc* in-frame deletion mutants were generated using previously described methods (He *et al*., 2006). The procedure was briefly described in Supporting Information. The primers used are listed in Table S3.

4.3 | Point mutagenesis of target gene in plasmid DNA and in Xcc chromosome

Point mutagenesis of target genes in plasmid DNA was conducted using the QuikChange Site-Directed Mutagenesis Kit following the manufacturer's instructions. The procedure was briefly described in Supporting Information. The primers used are listed in Table S3.

4.4 | Extraction and quantitative analysis of 2-HBA, 3-HBA and 4-HBA levels in plant leaf tissues

Cabbage (Jingfeng-1) and Chinese radish (Manshenhong) were grown in a greenhouse at 25°C and 75% humidity with a photoperiod of 16 h (8,000 Lx) for 2 months. After XC1 inoculation, the plants were transferred into a growth cabinet (NINBO YANGHUI, RND-400B) at 28°C and 90% humidity with a photoperiod of 16 h (8,000 Lx). Two hundred milligrams of the leaf tissues (2.5 cm × 2.5 cm) were collected from the leaves treated with XC1 strain or 1 × PBS buffer. 2-HBA, 3-HBA and 4-HBA were extracted from the leave tissues following the method established previously developed (Pan *et al*., 2010). The dry extracts were dissolved in 50 μL of methanol. Commercially available 2-HBA, 3-HBA and 4-HBA were purchased from Sigma (USA) and five reference solutions containing serially diluted standards were used to plot standard curves for quantitative analysis of endogenous levels of 2-HBA, 3-HBA and 4-HBA.

Ten-microliter extracts were loaded into the Ultra-High Performance Liquid Chromatography coupled with Triple Quadrupole Tandem Mass Spectrometry (UHPLC-QqQ-MS/MS) (Agilent, USA) for quantitative analysis. Chromatographic separation was carried out at 25°C on a Zorbax Eclipse XDB C18 column (4.6 × 150 mm, 5 μm, Agilent). The column was eluted with 0.1% formic acid water and 0.1% formic acid methanol (60/40, vol/vol) over 40 min at a flow rate of 0.4 mL min^{-1}. Quantitative analysis was performed using a triple quadrupole tandem mass spectrometer equipped with an electrospray ion source (ESI) (Agilent). The MS spectra were acquired in multiple reaction monitoring (MRM) mode. The fragmentor, collision energy and the precursor and product ions screened were all optimized for each compound using Agilent optimizer software. The optimal MS instrumental parameters were as follows: capillary voltage, 3.5 kV; gas temperature, 300°C; gas flow, 5 L min^{-1}; nebulizer, 45 psi; sheath gas temperature, 250°C, sheath gas flow, 11 L min^{-1}.

4.5 | Extraction and quantitative analysis of 4-HBA in XC1 cultures by high performance liquid chromatography (HPLC)

4-HBA in XC1 cultures was extracted and quantitatively analyzed as described previously (Zhou *et al*., 2013). Briefly, 0.5 mL of XC1 cultures at different time points were collected and adjusted to pH 3.5. One mL of ethyl acetate was used to extract 4-HBA. After evaporation, the dry crude extract was dissolved in 200 μL methanol, and 5 μL was taken for HPLC analysis. The 4-HBA level was quantified using the peak area for the HPLC eluate following the established formula as described previously (Zhou *et al*., 2013).

4.6 | Construction of gusA-dependent reporter strains to monitor pobA or pobR transcriptional activities

A 539-bp DNA fragment upstream of the translation initiation codon of *pobA* gene was amplified by PCR using XC1 genomic DNA as template and the primer set P_{pobA}-F/R (Table S3). A 484-bp DNA fragment upstream of the translation initiation codon of *pobR* gene was amplified using the primer set P_{pobR}-F/R (Table S3). Both PCR products were, respectively, cloned into the BamHI and HindIII sites of the plasmid pMD18T-T0T1-*gusA*, which contains a T0T1 terminator and a promoterless *gusA* reporter gene (Zhao *et al*., 2014). DNA fusion fragments harboring T0T1 terminator, *pobA* or *pobR* promoter region and *gusA* gene were amplified by PCR using the primer set T0T1-F and *gusA*-R (Table S3). The fusion genes were cloned into the SmaI and KpnI sites of mini-Tn7T-Gm plasmid (Choi and Schweizer, 2006) to generate plasmid mini-Tn7-T0T1-P_{pobA}-*gusA* or mini-Tn7-T0T1-P_{pobR}-*gusA*. The resultant plasmids were, respectively, integrated into XC1 by electroporation as described previously (Choi and Schweizer, 2006). GUS activity assay was conducted as described in Supporting Information.

4.7 | Total RNA extraction and qRT-PCR for transcription analysis

The total RNA of *Xcc* strains was isolated using the RNeasy Miniprep Kit (Qiagen). The PrimeScript RT reagent kit with gDNA Eraser was used for removing the genomic DNA and cDNA synthesis (Takara). Quantitation of *pobA* expression and melting curve analysis were performed using Mastercycler ep Realplex 4S (Eppendorf) with SYBR Premix Ex Taq (Takara). The *atpD* gene was used as reference to standardize all samples and replicates. The primers used are listed in Table S3.

4.8 | Protein expression and purification

The *pobR* coding region was amplified with the primers listed in Table S3 and fused to the expression vector pMAL-c2x (NEB). The fusion gene construct was transformed into the *E. coli* strain BL21 (DE3) to generate a new strain named BL21/pMAL-*pobR*. The detailed protocol for protein expression and purification was described in Supporting Information. The eluted proteins were, respectively, dissolved in two types of buffers. Buffer A contains 25 mM Tris, 300 mM NaCl, 2 mM EDTA and pH8.0, which is recommend by the

manufacturer NEB; buffer B contains 25 mM HEPES, 100 mM NaCl, 100 mM $MgCl_2$, 100 mM $(NH_4)_2SO_4$ and pH7.2.

4.9 | Electrophoretic mobility shift assay (EMSA) and DNase I footprinting sequencing assay

EMSA were performed according to the method described previously (Sun *et al*., 2017). The 233-bp DNA probe corresponding to the sequence from −207 to 26 bp in the overlapping region upstream of the *pobA* gene (P_A for short in this study) was amplified by PCR using the primer set Cy5-P_{pobA}-F/R (Table S3). Both the forward and reverse primers contain a universal DNA sequence (5′ AGCCAGTGGCGATAAG 3′) at the 5′ end. The probes were subsequently labeled via a second round of PCR by the Cy5-labeled universal sequence described above. Cy5-labeled probes P_A were incubated with PobR-MBP at a range of concentrations in EMSA buffer (20 mM Tris pH 7.9, 2 mM DTT, 10 mM $MgCl_2$, 5% glycerol, 40 μg mL^{-1} BSA, 100 ng mL^{-1} sonicated salmon sperm DNA). To verify the specificity of the interaction, 2000 ng of unlabeled P_A probe was amplified and added as a specific competitor. After incubation at 25°C for 20 min, the reaction mixture was electrophoresed at 4°C on a 4.5% native polyacrylamide gel in 0.5 × Tris-borate-EDTA (TBE) buffer for 45 min at 125 V. All the gels were pre-run in 0.5 × TBE buffer (120 V for 30 min). The gels were scanned for fluorescent DNA using the Starion FLA-9000 Scanner (FujiFilm, Japan).

DNase I footprinting sequencing assay were performed following a protocol described previously (Wang *et al*., 2012). The detailed protocol was described in Supporting Information.

4.10 | Isothermal titration calorimetry analysis

Isothermal titration calorimetry assays were performed on a MicroCal iTC200 system (GE Healthcare, USA). All the proteins and phenolic acids were freshly prepared in buffer B (25 mM HEPES, 100 mM NaCl, 100 mM $MgCl_2.6H_2O$, 100 mM $(NH_4)_2SO_4$, pH = 7.2). In a typical experiment, 50 μM protein was loaded into the sample cell and titrated against 400 μM phenolic acids in the injection syringe. Titrations were carried out at 18°C, and the stirring speed was 750 r.p.m. Data were analyzed using the Origin 7.0 software package provided by the manufacturer.

4.11 | Western blotting analysis

The proteins separated by SDS–PAGE were electrotransferred onto a PVDF membrane (Roche, USA). After blocking with 5% nonfat milk powder, the proteins were incubated with the 1:5,000 diluted anti-flag-tag mouse monoclonal antibody (Abmart, #M20008) as a primary antibody. The membrane was subsequently washed four times with TBST buffer (20 mM Tris, 0.15 M NaCl, 0.1% Tween 20(v/v)). The 1:6,500 diluted horseradish peroxidase (HRP) conjugated goat antimouse IgG (Abmart, #M21001) was used as secondary antibody. The monoclonal antibody against the α subunit of RNA polymerase (NeoClone) was used as a control for sample loading. After washing the membrane four times, a luminescent signal was detected by a ChampChemi 610 Plus (Sage Creation Science, China).

4.12 | Mapping of the pobA and pobR transcription starting site

The transcriptional start sites of *pobA* and *pobR* were identified with the 5′-Rapid Amplification of cDNA Ends (RACE) system (Invitrogen). Briefly, total RNA was extracted and purified using the RNeasy Mini Kit (Qiagen) from XC1 grown in XYS medium treated with 0.1 mM 4-HBA to elevate the levels of the *pobA* and *pobR* transcripts. The cDNA synthesis was performed using 20 pmol of primers (Table S3) and 2 μg of total RNA template according to the manufacturer's protocol. After cDNA synthesis, a RNase mixture was added into the reaction mix to remove the RNA template. An oligo-dC tail was added to the purified cDNA using the tailing reaction. dC-tailed cDNA was amplified using 2.5 μL of the preceding reaction mixture as template, the abridged anchor primer supplied with the kit and *Taq* DNA polymerase. The purified PCR product was then cloned into the pGEM-T Easy vector and transformed into the *E. coli* strain. The recombinant plasmid was prepared, and the cloned inserts were sequenced by BGI (Shanghai, China).

4.13 | Plant GUS histochemical staining assay and determination of bacterial growth in planta

All *Xcc* strains were cultured in NYG liquid medium overnight and adjusted to an OD_{600} of 0.1 (1.0×10^8 CFU mL^{-1}). The latter strains were subsequently inoculated into Chinese radish leaves using the leaf clipping method. At 3- and 5-days post inoculation, the infected leaves were collected for GUS histochemical staining using x-Gluc as a substrate (Li *et al*., 2014). The cell numbers inside the infected leaves and GUS activity analysis were measured in a parallel experiment following the protocol described by Vojnov *et al*. (2001). Briefly, three 0.9 cm^2 leaf disks were collected from the infiltrated area and homogenized in 3 mL of NYG liquid medium. Diluted homogenates were plated on NYG agar plates supplemented with 50 μg mL^{-1} Rif. Bacterial colony formation unit (CFU) was counted after incubation at 28°C for 3 days. GUS activity in the infected plant tissues was quantified using 4-methylumbelliferyl-β-D-glucuronide as the substrate. GUS activity values per 10^8 CFU are the means of three independent measurements. The XC1 strain carrying a promoterless *gusA* gene (XC1::*gusA*) and the previously constructed *hrpX* reporter strain *Xcc*(P_{hrpX}-*gusA*) (Li *et al*., 2014) were used as negative and positive control strains respectively.

4.14 | Virulence assay in Chinese radish and cabbage

The virulence of *Xcc* in Chinese radish (*Raphanus sativus* "Mangshenhong") or cabbage (Jingfeng-1) was tested by the leaf-clipping method. Leaves were cut with sterile scissors dipped in the requisite bacterial suspensions with OD_{600} values of 0.1 (1×10^8 CFU mL^{-1}). Lesion length was measured 2 weeks post inoculation. For each strain, a total of 15 leaves were inoculated and the average lesion lengths with standard deviation are shown.

4.15 | Statistical analysis

All experiments were performed at least three times. ANOVA for experimental data sets was performed using JMP software version 5.0 (SAS Institute Inc., Cary, NC). Significant effects of treatment were determined by the F value ($p = 0.05$). When a significant F test was obtained, separation of means was accomplished by Fisher's protected LSD (least significant difference) test at $p < 0.05$.

ACKNOWLEDGMENT

This work was financially supported by research grants from the National Key R&D Program of China (2017YFD0200900 to ZL) and the National Natural Science Foundation of China (No. 31972231 to HYW, No. 31772121 to HYW).

CONFLICT OF INTEREST

The authors declare no conflict of interest.

AUTHOR CONTRIBUTIONS

He and Tang conceived the experimental design, interpreted the results and wrote the manuscript. Chen, Li and Qiu performed the experiments. Song developed the assay method for promoter analysis.

ORCID

Ya-Wen He https://orcid.org/0000-0002-7349-924X

REFERENCES

Bertani, I., Kojic, M. and Venturi, V. (2001) Regulation of the *p*-hydroxybenzoic acid hydroxylase gene (*pobA*) in plant-growth-promoting *Pseudomonas putida* WCS358. *Microbiology*, *147*, 1611–1620.

Browning, D.F. and Busby, S.J. (2004) The regulation of bacterial transcription initiation. *Nature Reviews Microbiology*, *2*, 57–65.

Browning, D.F. and Busby, S.J.W. (2016) Local and global regulation of transcription initiation in bacteria. *Nature Reviews Microbiology*, *14*, 638–650.

Büttner, D. and Bonas, U. (2010) Regulation and secretion of *Xanthomonas* virulence factors. *FEMS Microbiology Reviews*, *34*, 107–133.

Choi, K.H. and Schweizer, H.P. (2006) Mini-Tn7 insertion in bacteria with single attTn7 sites: example *Pseudomonas aeruginosa*. *Nature Protocols*, *1*, 153–161.

Dimarco, A.A. and Ornston, L.N. (1994) Regulation of *p*-hydroxybenzoate hydroxylase synthesis by PobR bound to an operator in *Acinetobacter calcoaceticus*. *Journal of Bacteriology*, *176*, 4277–4284.

Donoso, R.A., Pérez-Pantoja, D. and González, B. (2011) Strict and direct transcriptional repression of the *pobA* gene by benzoate avoids 4-hydroxybenzoate degradation in the pollutant degrader bacterium *Cupriavidus necator* JMP134. *Environmental Microbiology*, *13*, 1590–1600.

Fuchs, G., Boll, M. and Heider, J. (2011) Microbial degradation of aromatic compounds–from one strategy to four. *Nature Reviews Microbiology*, *9*, 803–816.

Glazebrook, J. and Ausubel, F.M. (1994) Isolation of phytoalexin-deficient mutants of *Arabidopsis thaliana* and characterization of their interactions with bacterial pathogens. *Proceedings of the National Academy of Sciences of the United States of America*, *91*, 8955–8959.

Grüninger, M.J., Buchholz, P.C.F., Mordhorst, S., Strack, P., Müller, M., Hubrich, F., *et al.* (2019) Chorismatases –the family is growing. *Organic & Biomolecular Chemistry*, *17*, 2092–2098.

Harwood, C.S. and Parales, R.E. (1996) The *β*-ketoadipate pathway and the biology of self-identity. *Annual Review of Microbiology*, *50*, 553–590.

He, Y.W., Xu, M., Lin, K., Ng, Y.J.A., Wen, C.M., Wang, L.H., *et al.* (2006) Genome scale analysis of diffusible signal factor regulon in *Xanthomonas campestris* pv. *campestris*: identification of novel cell-cell communication-dependent genes and functions. *Molecular Microbiology*, *59*, 610–622.

Hugouvieux, V., Barber, C.E. and Daniels, M.J. (1998) Entry of *Xanthomonas campestris* pv. *campestris* into hydathodes of *Arabidopsis thaliana* leaves: a system for studying early infection events in bacterial pathogenesis. *Molecular Plant-Microbe Interactions*, *11*, 537–543.

Jung, D.H., Kim, E.J., Jung, E., Kazlauskas, R.J., Choi, K.Y. and Kim, B.G. (2016) Production of *p*-hydroxybenzoic acid from *p*-coumaric acid by *Burkholderia glumae* BGR1. *Biotechnology and Bioengineering*, *113*, 1493–1503.

Kok, R.G., D'Argenio, D.A. and Ornston, L.N. (1998) Mutation analysis of PobR and PcaU, closely related transcriptional activators in *Acinetobacter*. *Journal of Bacteriology*, *180*, 5058–5069.

Li, R.F., Lu, G.T., Li, L., Su, H.Z., Feng, G.F., Chen, Y., *et al.* (2014) Identification of a putative cognate sensor kinase for the two-component response regulator HrpG, a key regulator controlling the expression of the *hrp* genes in *Xanthomonas campestris* pv. *campestris*. *Environmental Microbiology*, *16*, 2053–2071.

Mansfield, J., Genin, S., Magori, S., Citovsky, V., Sriariyanum, M., Ronald, P., *et al.* (2012) Top 10 plant pathogenic bacteria in molecular plant pathology. *Molecular Plant Pathology*, *13*, 614–629.

Ni, L.S., Tonthat, N.K., Chinnam, N. and Schumacher, M.A. (2013) Structures of the *Escherichia coli* transcription activator and regulator of diauxie, XylR: an AraC DNA-binding family member with a LacI/GalR ligand-binding domain. *Nucleic Acids Research*, *41*, 1998–2008.

Pan, X.Q., Welti, R. and Wang, X.M. (2010) Quantitative analysis of major plant hormones in crude plant extracts by high-performance liquid chromatography-mass spectrometry. *Nature Protocols*, *5*, 986–992.

Quinn, J.A., Mckay, D.B. and Entsch, B. (2001) Analysis of the *pobA* and *pobR* genes controlling expression of *p*-hydroxybenzoate hydroxylase in *Azotobacter chroococcum*. *Gene*, *264*, 77–85.

Romero-Silva, M.J., Méndez, V., Agulló, L. and Seeger, M. (2013) Genomic and functional analyses of the gentisate and protocatechuate ring-cleavage pathways and related 3-hydroxybenzoate and 4-hydroxybenzoate peripheral pathways in *Burkholderia xenovorans* LB400. *PLoS ONE*, *8*, e56038.

Saecker, R.M., Record, M.T. Jr and deHaseth, P.L. (2011) Mechanism of bacterial transcription initiation: RNA polymerase–promoter binding, isomerization to initiation-competent open complexes, and initiation of RNA synthesis. *Journal of Molecular Biology*, *412*, 754–771.

Sircar, D. and Mitra, A. (2008) Evidence for *p*-hydroxybenzoate formation involving enzymatic phenylpropanoid side-chain cleavage in hairy roots of *Daucus carota*. *Journal of Plant Physiology*, *165*, 407–414.

Su, H.Z., Wu, L., Qi, Y.H., Liu, G.F., Lu, G.T. and Tang, J.L. (2016) Characterization of the GntR family regulator HpaR1 of the crucifer black rot pathogen *Xanthomonas campestris* pathovar *campestris*. *Scientific Reports*, *6*, 19862.

Sun, S., Chen, B., Jin, Z.J., Zhou, L., Fang, Y.L., Thawai, C., *et al*. (2017) Characterization of the multiple molecular mechanisms underlying RsaL control of phenazine-1-carboxylic acid biosynthesis in the rhizosphere bacterium *Pseudomonas aeruginosa* PA1201. *Molecular Microbiology*, *104*, 931–947.

Tan, J.W., Bednarek, P., Liu, J.K., Schneider, B., Svatos, A. and Hahlbrock, K. (2004) Universally occurring phenylpropanoid and species-specific indolic metabolites in infected and uninfected *Arabidopsis thaliana* roots and leaves. *Phytochemistry*, *65*, 691–699.

Timilsina, S., Potnis, N., Newberry, E.A., Liyanapathiranage, P., Iruegas-Bocardo, F., White, F.F., *et al*. (2020) *Xanthomonas* diversity, virulence and plant–pathogen interactions. *Nature Reviews Microbiology*, *18*, 415–427.

Tropel, D. and van der Meer, J.R. (2004) Bacterial transcriptional regulators for degradation pathways of aromatic compounds. *Microbiology and Molecular Biology Reviews*, *68*, 474–500.

Venturi, V., Zennaro, F., Degrassi, G., Okeke, B.C. and Bruschi, C.V. (1998) Genetics of ferulic acid bioconversion to protocatechuic acid in plant-growth-promoting *Pseudomonas putida* WCS358. *Microbiology*, *144*, 965–973.

Vicente, J.G. and Holub, E.B. (2013) *Xanthomonas campestris* pv. *campestris* (cause of black rot of crucifers) in the genomic era is still a worldwide threat to brassica crops. *Molecular Plant Pathology*, *14*, 2–18.

Vojnov, A.A., Slater, H., Daniels, M.J. and Dow, J.M. (2001) Expression of the *gum* operon directing xanthan biosynthesis in *Xanthomonas campestris* and its regulation in planta. *Molecular Plant-Microbe Interactions*, *14*, 768–774.

Wang, J.Y., Zhou, L., Chen, B., Sun, S., Zhang, W., Li, M., *et al*. (2015) A functional 4-hydroxybenzoate degradation pathway in the phytopathogen *Xanthomonas campestris* is required for full pathogenicity. *Scientific Reports*, *5*, 18456.

Wang, Y., Cen, X.F., Zhao, G.P. and Wang, J. (2012) Characterization of a new GlnR binding box in the promoter of *amtB* in *Streptomyces coelicolor* inferred a PhoP/GlnR competitive binding mechanism for transcriptional regulation of *amtB*. *Journal of Bacteriology*, *194*, 5237–5244.

Zhang, R., Lord, D.M., Bajaj, R., Peti, W., Page, R. and Sello, J.K. (2018) A peculiar IclR family transcription factor regulates *para*-hydroxybenzoate catabolism in *Streptomyces coelicolor*. *Nucleic Acids Research*, *46*, 1501–1512.

Zhao, Z.H., Xiong, L., Shen, C.W., Sun, Q.B., Zou, L.F. and Chen, G.Y. (2014) Construction of two promoter-probe vectors suitable for pathogenicity-related gene expression analysis in *Xanthomonas oryzae* pv. *oryzicola*. *Acta Phytopathologica Sinica*, *44*, 504–511.

Zhou, L., Wang, J.Y., Wang, J.H., Poplawsky, A., Lin, S.J., Zhu, B.S., *et al*. (2013) The diffusible factor synthase XanB2 is a bifunctional chorismatase that links the shikimate pathway to ubiquinone and xanthomonadins biosynthetic pathways. *Molecular Microbiology*, *87*, 80–93.

Zhou, L., Zhang, L.H., Camara, M. and He, Y.W. (2017) The DSF family of quorum sensing signals: diversity. Biosynthesis and Turnover. *Trends in Microbiology*, *25*, 293–303.

SUPPORTING INFORMATION

Additional Supporting Information may be found online in the Supporting Information section.

How to cite this article: Chen B, Li R-F, Zhou L, et al. The phytopathogen *Xanthomonas campestris* utilizes the divergently transcribed *pobA*/*pobR* locus for 4-hydroxybenzoic acid recognition and degradation to promote virulence. *Mol Microbiol*. 2020;114:870–886. https://doi.org/10.1111/mmi.14585